ON THE EXISTENCE OF HYSTERESIS IN THE KURAMOTO MODEL WITH BIMODAL FREQUENCY DISTRIBUTIONS

DIEGO PAZÓ AND ERNEST MONTBRIÓ

Abstract. We investigate the transition to synchronization in the Kuramoto model with bimodal distributions of the natural frequencies. Previous studies have concluded that the model exhibits a hysteretic phase transition if the bimodal distribution is close to a unimodal one, due to the shallowness the central dip. Here we show that proximity to the unimodal-bimodal border does not necessarily imply hysteresis when the width, but not the depth, of the central dip tends to zero. We draw this conclusion from a detailed study of the Kuramoto model with a suitable family of bimodal distributions.

1. Introduction

Understanding the dynamics of large populations of heterogeneous self-sustained oscillatory units is of great interest because they occur in a wide range of natural phenomena and technological applications [1]. Often a macroscopic system self-organizes into a synchronous state, in which a certain fraction of its units acquires a common frequency. This occurs as a consequence of the mutual interactions among the oscillators and despite the differences in their rhythms [2]. Examples of collective synchronization include pacemaker cells in the heart and nervous system [3, 4], synchronously flashing fireflies [5], collective oscillations of pancreatic beta cells [6] and pedestrian induced oscillations in bridges [7].

A fundamental contribution to the study of collective synchronization was the model proposed by Kuramoto [8]. This model, and a large number of extensions of it, has been extensively studied because it is analytically tractable but still captures the essential dynamics of collective synchronization phenomena (for reviews see [9, 1, 10, 11]). The original Kuramoto model consists of a population of N oscillators interacting all to all. The state of an oscillator i is described by its phase $\theta_i(t)$ that evolves in time according to

$$\dot{\theta}_i = \omega_i - \frac{K}{N}\sum_{j=1}^{N}\sin(\theta_i - \theta_j). \tag{1}$$

The parameter K determines the strength of the interaction between one oscillator and another. The oscillators are considered to have different natural

Date: October 5, 2009.

frequencies ω_i, that are taken from a probability distribution $g(\omega)$. In his analysis Kuramoto adopted the thermodynamic limit $N \to \infty$ and considered $g(\omega)$ to be symmetric. In this case, and without loss of generality, the distribution can always be centered at zero, *i.e.* $g(\omega) = g(-\omega)$, by going into a rotating framework $\theta_j \to \theta_j + \Omega t$.

Kuramoto found useful to study the synchronization dynamics of system (1) in terms of a complex order parameter $z = N^{-1} \sum_{j=1}^{N} \exp(i\ \theta_j)$. Note that z is a mean field that indicates the onset of coherence due to synchronization in the population. System (1) possesses an incoherent state with $z = 0$ (that exists for all values of the coupling strength K) in which the oscillators rotate independently as if they were uncoupled, $\theta_i(t) \sim \omega_i t$. Using a self-consistency argument, Kuramoto found that for a unimodal distribution $g(\omega)$, above the coupling's critical value

$$K_c = \frac{2}{\pi g(0)}, \tag{2}$$

a new solution with asymptotics

$$|z| \approx \frac{4}{K_c^2} \sqrt{\frac{K - K_c}{-\pi g''(0)}} \tag{3}$$

branches off the incoherent ($z = 0$) solution. This emerging solution is a *partially synchronized* (PS) state, in which a subset of the population S entrains to the central frequency ($\theta_{i \in S} = \text{const.}$).

Equation (3) shows that the orientation of the PS bifurcating branch depends on whether the distribution is concave or convex at its center. As a consequence of that, at $K = K_c$ the PS state is expected to bifurcate supercritically for unimodal distributions ($g''(0) < 0$) and subcritically for bimodal distributions ($g''(0) > 0$). However, Kuramoto's analysis did not permit to study the stability of the solutions and thus one cannot conclude whether bimodal distributions show bistability close to the transition point (2) (see discussion in p. 75 of [8]). In fact, Kuramoto discarded the possibility of bistability. Instead he expected the incoherent state to become unstable earlier, *i.e.* at a certain critical value $K_c' < K_c$, via the formation of two symmetric clusters of synchronized oscillators near the distribution's maxima (later Crawford called this state *standing wave* (SW) [12]). As the coupling is increased further, he predicted that the interaction between the clusters would tend to synchronize them forming a single synchronized group, *i.e.* a PS state.

1.1. **Sum of unimodal distributions with different mean.**

After Kuramoto's seminal work [8], several articles have further investigated the synchronization transition in model (1) with symmetric bimodal distributions [14, 12, 15, 16, 17, 13]. These studies assumed $g(\omega)$ to be the superposition of two identical even

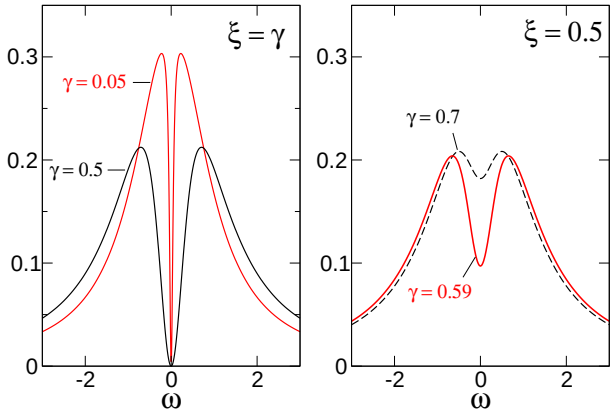

FIGURE 1. (Color online) Examples of bimodal frequency distributions given by Eq. (5) with $\delta = 1$. Left panel: $\xi = \gamma$ (what implies $g(0) = 0$). Note that as γ decreases the maxima of the distribution become closer. For *all* these distributions (with $\xi = \gamma$) the route to synchronization as K is increased from zero is I→SW→PS, c.f. Fig. 3. Right panel: Two examples with $\xi < \gamma$. The distribution depicted with a continuous line has well separated peaks and shows a transition I→SW→PS, whereas the other distribution is closer to the unimodal limit (7) and presents hysteresis in the route to synchronization, c.f. Fig. 4.

unimodal distributions $\tilde{g}(\omega)$ centered at $\pm\omega_0$: $g(\omega) = \tilde{g}(\omega + \omega_0) + \tilde{g}(\omega - \omega_0)$ [1]. Parameter ω_0 controls the separation of the peaks. Decreasing ω_0 the distribution's maxima approach each other and, at the same time, the central distribution's dip becomes shallower (*i.e.* $g(0)$ increases). Eventually, at a value $\omega_0 = \omega_{0B}$ that satisfies

$$g''(\omega = 0)|_{\omega_0 = \omega_{0B}} = 0. \tag{4}$$

the peaks merge and the distribution becomes unimodal. The dynamics of the Kuramoto model for distributions of this type is as follows [13]: When the peaks are well separated (ω_0 larger than a certain value ω_{0D}) the transitions increasing K are as Kuramoto foresaw: Incoherence → SW → PS. However, if the peaks are near ($\omega_{0D} > \omega_0 > \omega_{0B}$) there exists a range of K below K_c where bistability between incoherence and either a PS or a SW state is observed, as Eq. (3) suggested [2].

[1]The choice $\tilde{g}$ to be of Lorentzian (Cauchy) type is popular because the mathematics usually simplifies. Some works however investigate a population consisting of two groups of identical oscillators [$\tilde{g}(\omega) = \delta(\omega)$] with model (1) in the presence of noise [14, 15].

[2]Similar results have been obtained studying the interaction between populations with Lorentzian frequency distributions [18, 19]. In this context the bimodal distribution arises naturally as the superposition the two unimodal distributions.

1.2. **Difference of unimodal distributions with different width.** In this article we are interested in understanding the synchronization transition in the Kuramoto model with bimodal distributions in situations that cannot be achieved summing even unimodal distributions. In particular summing even distributions implies that if the peaks are brought closer the central dip becomes less deep (unless the distributions are Dirac deltas). Thus we cannot approach the peaks arbitrarily near while keeping the central dip's depth (see *e.g.* in the left panel of Fig. 1 for a distribution family with constant depth but arbitrary distance between the peaks).

We will use a family of bimodal distributions that are constructed as the difference of two unimodal even functions with the same mean and different widths: $g(\omega) = \tilde{g}_1(\omega) - \tilde{g}_2(\omega)$. These distributions could be useful to model systems in which a fraction of the central natural frequencies of a population $\tilde{g}_1$ is missing due to for example, some resonance, symmetry, or external disturbance.

We choose the functions $\tilde{g}_i$ to be Lorentzians, because of their mathematical tractability. Assuming $\delta > \gamma$ the normalized distribution reads

$$g(\omega) = \frac{\Xi}{\pi}\left[\frac{\delta^2}{\omega^2+\delta^2} - \xi\left(\frac{\gamma}{\omega^2+\gamma^2}\right)\right] \tag{5}$$

with $\xi \leq \gamma$ to be well defined, and $\Xi = 1/(\delta - \xi)$ is the normalization constant. Without loss of generality we assume $\delta = 1$ hereafter, because this can be always achieved rescaling ω, time and the parameters: $\omega' = \omega/\delta$, $t' = t\delta$, $K' = K/\delta$, $\gamma' = \gamma/\delta$ and $\xi' = \xi/\delta$. We will also drop the primes to lighten the notation. Figure 1 shows several examples of distributions (5). Distribution family (5) can exhibit an arbitrarily deep minimum while keeping the maxima as near as wished.

The left panel of Fig. 1 shows two examples for the case $\xi = \gamma$, which will be analyzed in detail below. This case implies $g(0) = 0$, which corresponds to the maximal value of the ratio $\xi/\gamma = 1$. As $\gamma \to 0$, the central dip becomes infinitely narrow and at $\gamma = 0$ the distribution becomes unimodal. This unimodal transition is therefore discontinuous and satisfies [3]:

$$\lim_{\gamma\to 0^+} g''(\omega = 0) = \infty, \tag{6}$$

In addition, distribution (5) also presents the regular unimodal-bimodal border via $g''(0) = 0$ at

$$\xi_B = \gamma^3 \tag{7}$$

with $\gamma \neq 0$ (line B in Fig. 2).

The outline of the paper is as follows: Section 2 summarizes recent theoretical results that permit to reduce the Kuramoto model to a system of ordinary differential equations with complex variables. These results are then used to find

[3] $g''(0) \sim \xi/\gamma^3$ diverges as $\xi \leq \gamma \to 0$ if $\xi = O(\gamma^a)$ with $a < 3$, *e.g.* $\xi = \gamma$ ($a = 1$).

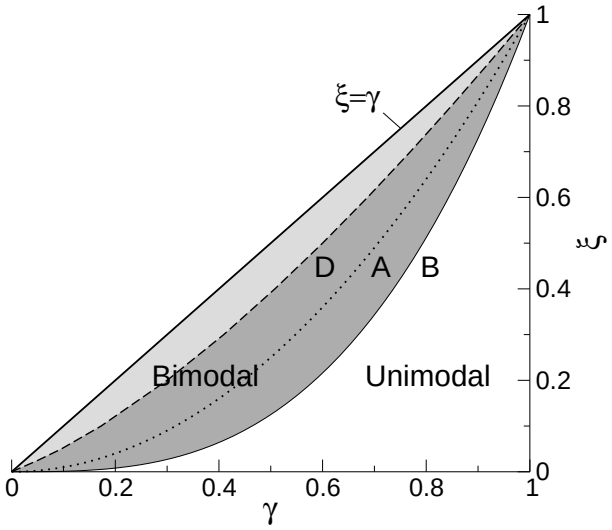

FIGURE 2. The parameter space of distribution (5) [not defined above the bisectrix $\xi = \gamma$ neither at point (1,1)]. Function (5) is unimodal below line B and bimodal above it (shaded regions). Three lines signal the loci of codimension-two bifurcations (A, B, and D) projected on the (γ, ξ) plane. Between lines D and B (dark grey region) the transition to synchronization involves hysteresis.

the two ODEs that describe the dynamics of the Kuramoto model with distribution (5). In Sec. 3 we study the special case $\xi = \gamma$, and we show that there indeed exists a transition to synchronization in absence of hysteresis independent on the separation between the distribution's maxima. Namely, in this case the route to synchronization is always: Incoherence→SW→PS. In Sec. 4 we study the most general case $g(0) > 0$, and determine the disposition of the different synchronization scenarios with respect to the unimodal-bimodal border.

2. Low dimensional description of the Kuramoto model

We start considering the thermodynamic limit $N \to \infty$ of model (1). We drop hence the indices in Eq. (1) and introduce the probability density for the phases $f(\theta, \omega, t)$ [8, 21]. Then $f(\theta, \omega, t)\, d\theta\, d\omega$ represents the ratio of oscillators with phases between θ and $\theta + d\theta$, and natural frequencies between ω and $\omega + d\omega$. The density function f obeys the continuity equation

$$\frac{\partial f}{\partial t} = -\frac{\partial (fv)}{\partial \theta}, \tag{8}$$

where, the angular velocity of the oscillators v is given by

$$v(\theta, \omega, t) = \omega - K \int_0^{2\pi} f(\theta', \omega, t) \sin(\theta - \theta') d\theta' \tag{9}$$

In the continuous formalism, the complex order parameter defined by Kuramoto becomes

$$z(t) = \int_{-\infty}^{\infty} \int_{0}^{2\pi} e^{i\theta} f(\theta, \omega, t)\, d\theta\, d\omega. \tag{10}$$

Since the density function $f(\theta, \omega, t)$ is real and 2π periodic in the θ variable, it admits the Fourier expansion

$$f(\theta, \omega, t) = \frac{g(\omega)}{2\pi} \left[1 + \sum_{n=1}^{\infty} \left(f_n(\omega, t) e^{in\theta} + \text{c.c.} \right) \right], \tag{11}$$

where $f_n = f_{-n}^*$. Note that the order parameter (10) now reduces to

$$z^*(t) = \int_{-\infty}^{\infty} g(\omega) f_1(\omega, t)\, d\omega. \tag{12}$$

Substituting the Fourier series (11) into the continuity equation (8), and using Eq. (12) one gets an infinite set of integro-differential equations for the Fourier modes

$$\dot{f}_n = -in\omega f_n + \frac{nK}{2} \left(z^* f_{n-1} - z f_{n+1} \right). \tag{13}$$

Recently Ott and Antonsen (OA) found a very remarkable result [22]: The ansatz

$$f_n(\omega, t) = \alpha(\omega, t)^n \tag{14}$$

is a particular –and usually the asymptotic– solution of the infinite set of Eqs. (13) if α satisfies

$$\dot{\alpha} = -i\omega\alpha + \frac{K}{2} \left(z^* - z\alpha^2 \right). \tag{15}$$

Equation (15) reduces to a finite set of ODEs for distributions $g(\omega)$ with a finite set of simple poles out of the real axis. Recalling $f_1 = \alpha$ the order parameter can be calculated by extending the integral in (12) to a contour integration in the complex plane. This is possible since α has an analytic continuation in the lower half ω-plane [22]. In turn only the values of α at the poles of $g(\omega)$ with negative imaginary part are relevant.

Several recent studies show that the ansatz (14) yields predictions in agreement with numerical simulations [22, 13, 23, 24, 25, 26, 27]. In addition Ott and Antonsen theoretically support the validity of their ansatz for the case of a Lorentzian distribution [28]. So far, disagreement between the OA ansatz and numerical results has been shown for frequency distributions with no spread and non-odd-symmetric coupling function. This entails the freedom to select arbitrary values for some constants of motion [29].

2.1. **Main Equations.** In this section we use the OA ansatz considering the frequency distribution (5). This yields two ODEs governing the dynamics inside the low-dimensional OA manifold. First of all, it is convenient to express (5) in partial fractions:

$$g(\omega) = \frac{\Xi}{2\pi i}\left(\frac{1}{\omega - i} - \frac{1}{\omega + i} - \frac{\xi}{\omega - \gamma i} + \frac{\xi}{\omega + \gamma i}\right). \tag{16}$$

Then, according to Eq. (12) the order parameter reads

$$z^*(t) = \Xi[\alpha_1(t) - \xi\alpha_2(t)], \tag{17}$$

with $\alpha_1(t) = \alpha(\omega = -i, t)$, and $\alpha_2(t) = \alpha(\omega = -i\gamma, t)$. Using (17) in Eq. (15), we obtain the following two ODEs with complex variables that govern the evolution of the order parameter (17)

$$\dot{\alpha}_1 = -\alpha_1 + k(\alpha_1 - \xi\alpha_2) - k(\alpha_1^* - \xi\alpha_2^*)\alpha_1^2 \tag{18a}$$

$$\dot{\alpha}_2 = -\gamma\alpha_2 + k(\alpha_1 - \xi\alpha_2) - k(\alpha_1^* - \xi\alpha_2^*)\alpha_2^2, \tag{18b}$$

with $k = \Xi K/2$. The phase space of Eqs. (18) is four dimensional, but due to the global phase shift invariance $(\alpha_1, \alpha_2) \to (\alpha_1 e^{i\beta}, \alpha_2 e^{i\beta})$ the dynamics is actually three dimensional [see also Eqs. (31) in Appendix A].

2.2. **Fixed points.** According to Eq. (17), the fixed points of Eqs. (18) correspond to steady states of the order parameter z. The trivial solution $\alpha_1 = \alpha_2 = 0$ yields $z = 0$, corresponding to the incoherent state.

In order to calculate the non-trivial fixed points, note first that invariance under the action of the global rotation $e^{i\beta}$ allows us to choose $\alpha_1 = x_1 + iy_1$ real, *i.e.* $\alpha_1 = x_1$. It follows from Eq. (18a) that the fixed points lie on the subspace where α_2 is real too. We can therefore take α_1 and α_2 as real (keeping in mind that a continuous of fixed points is generated under the action the neutral rotation $e^{i\beta}$). Hence, the equations for the fixed points are:

$$0 = -x_1 + k(x_1 - \xi x_2)(1 - x_1^2) \tag{19a}$$

$$0 = -\gamma x_2 + k(x_1 - \xi x_2)(1 - x_2^2) \tag{19b}$$

Additionally, note that these equations are symmetric under the reflection $(x_1, x_2) \to (-x_1, -x_2)$. This implies that the solutions (with the exception of the solution at the origin) exist always in pairs with opposite signs $(\pm x_1, \pm x_2)$.

Subtracting Eq. (19a) from Eq. (19b) multiplied by $\frac{\xi}{\gamma}$, we obtain $x_2^2 = \frac{\gamma}{\xi}[x_1^2 + \frac{1}{k} + \frac{\xi}{\gamma} - 1]$. This can be substituted back into Eq. (19a) to get a cubic equation

in $X \equiv x_1^2$:

$$\begin{aligned} P(X) &= k^2(1-\gamma\xi)X^3 \\ &- k\left[(2k-1)(1-\gamma\xi)-1+k\xi(\xi-\gamma)\right]X^2 \\ &+ \left[(k^2-2k)(1-\gamma\xi)+1+2k^2\xi(\xi-\gamma)\right]X \\ &- k\xi\left[\gamma+k(\xi-\gamma)\right]=0 \end{aligned} \tag{20}$$

Each of the solutions of this equation yields two twin solutions with coordinates

$$x_1 = \pm\sqrt{X} \qquad \xi x_2 = x_1[1-\tfrac{1}{k(1-X)}]. \tag{21}$$

After some algebra we obtain the relation of the solutions with order parameter:

$$|z| = \frac{2\,\xi\,\sqrt{X}}{K(1-X)}. \tag{22}$$

A steady state (x_1, x_2) results in a time-independent value of z and hence it should correspond to a partially synchronized state. However, note that X can only take values within the range $X \in [0, 1-2\frac{\xi}{K}[(\frac{\xi}{K}+1)^{1/2}-\frac{\xi}{K}]$ to have a z value consistent with its definition, *i.e.* $|z| \in [0,1]$.

As the polynomial in Eq. (20) is cubic, there is one real solution, $X_{(3)}$, for all the parameters values. This solution lays in the range $[0,1]$ (for $k>1$ a better bound is $[1-1/k, 1]$, since $P(1-1/k) = -\xi^2 < 0$ and $P(1) = 1 > 0$). However, it turns out that the fixed points associated to $X_{(3)}$ are 'unphysical' (even though in some parameter ranges $|z|<1$). The reason is that the x_2 coordinate, corresponding to the solution $X_{(3)}$, is always larger than 1 in absolute value. This implies $|\alpha_2| > 0$, and according to Eq. (14) the Fourier series of the density function $f(\theta, \omega, t)$ is divergent at $\omega = -i\gamma$.

We will see below that for large enough values of K there exist two more real solutions of $P(X)$: $X_{(1)} \leq X_{(2)} < 1-1/k$. In this case (except when $X_{(1)}$ becomes negative) such solutions indeed correspond to PS states of the original Kuramoto model (1).

3. Bimodal distributions vanishing at their center ($\xi = \gamma$)

In this section we consider $\xi = \gamma$ what implies that distribution (5) vanishes at its center, $g(0) = 0$. In this case γ (or ξ) becomes the parameter controlling the width of the central dip of $g(\omega)$, and the maxima of the distribution are located at (see Fig. 1, left panel):

$$\omega = \pm\gamma. \tag{23}$$

3.1. **Stability of the incoherent state.**

In the incoherent state the oscillators are uniformly distributed in the interval $[0, 2\pi)$, and thus the order parameter vanishes. This state corresponds to the fixed point at the origin $\alpha_1 = \alpha_2 = 0$. A linear stability analysis of Eqs. (18) reveals that this fixed point undergoes a

degenerate Hopf bifurcation at $k_H = (1+\gamma)/(1-\gamma)$. In terms of the original coupling constant K, we find

$$K_H = 2 + 2\gamma. \tag{24}$$

At this point the eigenvalues are imaginary $\lambda_{1,2} = \lambda_{3,4}^* = i\sqrt{\gamma}$ and two-fold degenerate. Observe that as $\gamma \to 0$, the critical coupling for a (unimodal) Lorentzian distribution of unit width is recovered: $K_H(\gamma \to 0) = K_c = 2/(\pi g(0)) = 2$. Figure 3 shows the boundary K_H in the (γ, K) plane. As expected, we find that as the central dip of the distribution broadens (increasing γ) the stability region of the incoherent state grows.

3.2. **Saddle-node bifurcation.** The cubic equation (20) for the non-trivial fixed points becomes greately simplified under the assumption $\xi = \gamma$:

$$\begin{aligned} Q(X) &= k^2(1-\gamma^2)X^3 - k\left[(2k-1)(1-\gamma^2) - 1\right]X^2 \\ &+ \left[(k^2-2k)(1-\gamma^2)+1\right]X - \gamma^2 k = 0. \end{aligned} \tag{25}$$

For $\gamma = 0$ the central dip vanishes, and we recover the solutions for a Lorentzian distribution $X = 0, 1 - 1/k$. When $\gamma > 0$ there is a saddle-node bifurcation at $k = k_{SN}$, *i.e.* there is a transition from one (for $k < k_{SN}$) to three solutions (for $k > k_{SN}$). k_{SN} and γ can be related imposing the condition that the discriminant of $Q(X)$ vanishes. This gives the following relation:

$$\gamma^2 = \frac{8k_{SN}^4 - (1+8k_{SN}^2)^{3/2} + 20k_{SN}^2 - 1}{8k_{SN}(k_{SN}+1)^3}. \tag{26}$$

There are two important asymptotic values for this bifurcation line, which expressed in terms of the original coupling constant K are

$$K_{SN}(\gamma \to 0) = 2 + 6\left(\frac{\gamma}{2}\right)^{2/3} + O(\gamma), \tag{27}$$

$$K_{SN}(\gamma \to 1) \simeq (3+\sqrt{8})\left(1 - \tfrac{1-\gamma}{2}\right). \tag{28}$$

When K increases above K_{SN} the born solutions depart from each other $X_{(2)} - X_{(1)} \sim \sqrt{K - K_{SN}}$ + h.o.t. One solution becomes progressively smaller $(dX_{(1)}(K)/dK < 0)$, whereas the second one grows $(dX_{(2)}(K)/dK > 0)$. The latter solution $X_{(2)}$ yields a monotonically growing value of $|z|$ with K. This is not surprising because in the Kuramoto model, at large values of K, there exists always a stable PS solution with $d|z|/dK > 0$ (and $\lim_{K\to\infty}|z| = 1$, *i.e.* full synchronization). We advance that the corresponding twin fixed points from $X_{(2)}$ are stable, whereas the fixed points corresponding to $X_{(1)}$ are saddle.

3.3. **Numerical simulations and phase diagram.** In this section we construct the phase diagram with the loci of Hopf and saddle-node bifurcations that we have obtained above. Numerical simulations of the reduced Eqs. (18) were carried out and compared with the full model (1). This permits to relate the

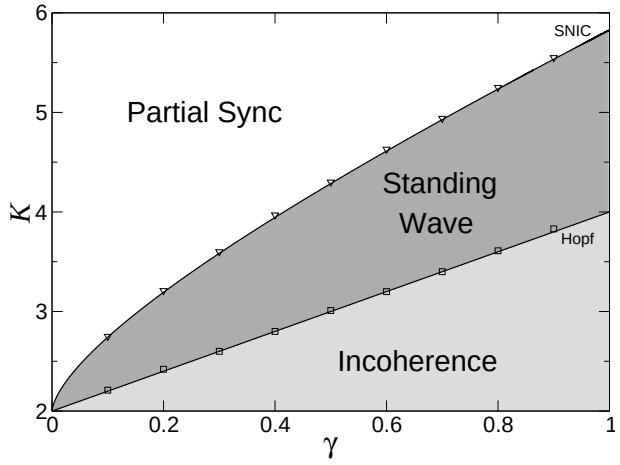

FIGURE 3. Phase diagram for $\xi = \gamma$. For this case the synchronization transition never involves hysteresis. The solid lines mark the saddle-node (SNIC) [from Eq. (26)] and the Hopf [Eq. (24)] bifurcations. Symbols correspond to the numerical estimation of the bifurcation lines via numerical integration of the original Eq. (1) with $N = 2000$.

dynamics of the variables $\alpha_{1,2}$ with the actual dynamical states of the Kuramoto model.

As already mentioned, the four-dimensional system (18) is effectively three-dimensional due to the existence of a neutral global rotation. Interestingly the attractors of the model are apparently embedded into a *two*-dimensional plane. Numerical simulations of Eqs. (18) using arbitrary initial conditions show that the dynamics always collapses into a plane which, by virtue of the neutral rotation $e^{i\beta}$, can be made coincident with the (x_1, x_2) plane, hereafter referred to as the "real plane". The stability against perturbations transversal to the real plane (and not tangent to the global rotation) is difficult to prove analytically. For the fixed point $X_{(2)}$ born at the saddle-node, the stability against transversal perturbations is proven in Appendix A. Other attractors (limit cycle) are transversally stable according to our numerical simulations.

Numerical simulations of the reduced Eqs. (18) with either real or complex variables, it is irrelevant, reveal that

(i) The Hopf bifurcation at $K = K_H$ is supercritical and it gives rise to a limit cycle around the origin. Due to the reflection symmetry of the equations $z(t)$ vanishes twice per period [this occurs when $\alpha_1 = \gamma\alpha_2$, see Eq. (17)]. It is therefore reasonable to assume that the limit cycle corresponds to the SW state, for which the two counter-rotating clusters of phase-locked oscillators are π out of phase twice per period.

(ii) The oscillatory dynamics appearing at K_H is destroyed at $K = K_{SN}$ where twin saddle-node bifurcations give rise to twin pairs of fixed points *on* the limit cycle. This bifurcation is known as SNIC (saddle-node on the invariant circle), or SNIPER (saddle-node infinite period). As K approaches K_{SN} from below the period of $|z(t)|$ diverges due to the slowing down of the dynamics at the twin bottlenecks anticipating the cease of oscillations via the (double) SNIC bifurcation.

Finally, numerical simulations of the full Kuramoto model (1) confirm the scenario I $\to$ SW $\to$ PS predicted by the reduced equations (18). We have numerically determined the boundaries of different behaviors: Square symbols in Fig. 3 are points in which the incoherent state loses stability leading to a SW state. Additionally, triangles indicate points where the order parameter becomes stationary.

3.4. **Concluding remarks.** Distribution (5) with $\xi = \gamma$ becomes unimodal only for $\gamma = 0$. As $\gamma \to 0$ the bimodal distribution tends to a unimodal, but the limit is nonregular. The remarkable point is that bistability is not observed, even if the central dip is extremely narrow ($\gamma \to 0$) . This is in sharp contrast with the scenario found when the peaks are close to merge with $g''(0) \to 0^+$ at the usual unimodal-bimodal transition (see below).

Another interesting fact is that the counter-rotating clusters of the SW are born at the Hopf bifurcation (24) with frequencies $\pm\sqrt{\gamma}$, although the maxima of the distribution are located at $\pm\gamma$. This means that the relative shift between distribution's maxima and cluster frequencies at the onset of the SW diverges as $\gamma \to 0$. This is a consequence of the extreme asymmetry of the peaks in this limit.

4. Bimodal distributions nonvanishing at their center ($\xi < \gamma$)

In this section we analyze the case $\xi < \gamma$, which is complementary to the one studied in the previous setion ($\xi = \gamma$). Thus, in the present case we let ξ and γ to be independent of each other (see Fig. 2). As we did in the previous section, we determine first the local bifurcations of the fixed points, and then we summarize our findings in the (γ, K) phase plane together with the results obtained by numerical integration of the reduced Eqs. (18) as well as of the full Kuramoto model (1).

4.1. **Fixed points.**

4.1.1. *The incoherent state and its stability.* The incoherent state becomes unstable in two possible ways depending on the value of ξ with respect to:

$$\xi_A = \gamma^2 \tag{29}$$

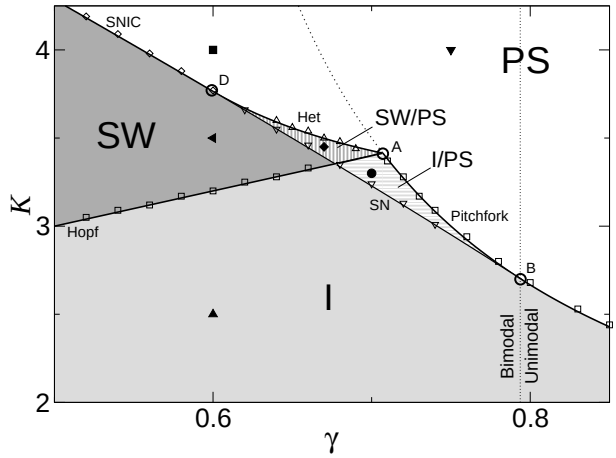

FIGURE 4. Phase diagram for $\xi = 0.5$. Solid lines mark the bifurcations: Saddle-node off the limit cycle (SN), SNIC, Hopf bifurcation [Eq. (24)], heteroclinic bifurcation (found numerically using the reduced equations), and pitchfork bifurcation [Eq. (30)]. Three big circles signal the codimension-two points: (A) Takens-Bogdanov, (B) degenerate pitchfork, (D) saddle-node separatrix-loop. The open symbols correspond to different bifurcations found by numerical integration of Eqs. (1) with $N = 2000$. Filled symbols inside each region indicate parameter values for the phase portraits in Fig. 5.

(see line A in Fig. 2). For $\xi < \xi_A$, there is a degenerate Hopf bifurcation at the critical value K_H given by Eq. (24) which is independent of ξ. For $\xi > \xi_A$, the instability of the incoherent state occurs via a pitchfork bifurcation at:

$$K_P = \frac{2}{\pi g(0)} = \frac{2\gamma(1-\xi)}{\gamma - \xi}. \tag{30}$$

The bifurcation is subcritical, and it switches to supercritical when the distribution becomes unimodal at $\gamma > \xi_B^{1/3}$. The loci of Hopf and pitchfork bifurcations collide at the codimension-two point where $K_H = K_P$ and $\xi = \xi_A$. This point is of the double zero eigenvalue type (Takens-Bogdanov) [30].

The boundaries (24) and (30) for Hopf and pitchfork instabilities have been also obtained following a different approach in Appendix B.

4.1.2. *Non-trivial fixed points (partial synchronization).* A saddle-node bifurcation occurs when $P(X)$ in Eq. (20) has exactly two roots (one of them two-fold degenerate). And this bifurcation point can be determined numerically finding the value of k where the discriminant of $P(X)$ vanishes. The scenario is similar to the one observed for $\xi = \gamma$, but in this case the saddle solution $X_{(1)} > 0$ exists

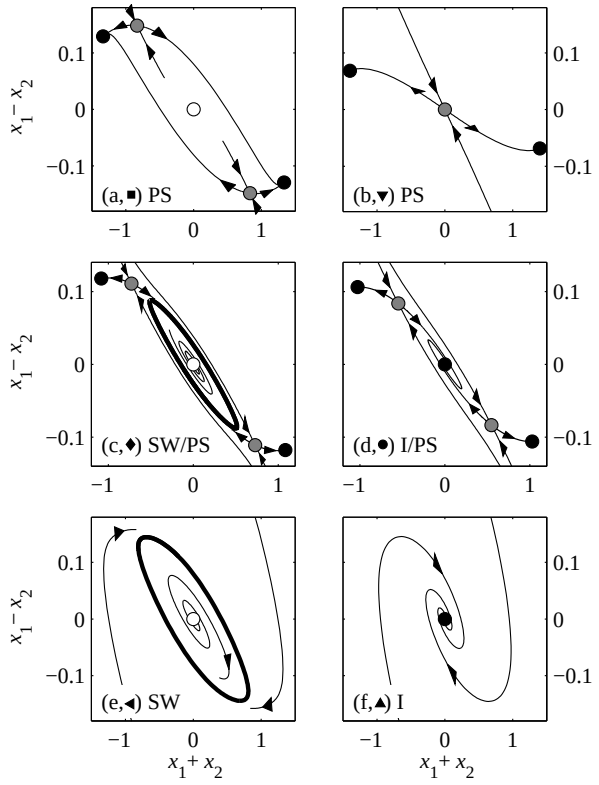

FIGURE 5. Phase portraits in (rotated) x_1, x_2 coordinates for qualitatively different cases. Each panel corresponds to a value of γ and K at the position of a filled symbol in Fig. 4. (a,b) Partial synchronization with $K = 4$, and (a) $\gamma = 0.6$ and (b) $\gamma = 0.75$; (c) Coexistence SW/PS: $\gamma = 0.67$, $K = 3.45$; (d) Coexistence I/PS: $\gamma = 0.7$, $K = 3.3$; (e) SW, $\gamma = 0.6$, $K = 3.5$; (f) I, $\gamma = 0.6$, $K = 2.5$.

up to the pitchfork bifurcation with the origin at $K = K_P$. If the distribution is unimodal $X_{(1)} < 0$ what makes this solution not valid.

4.2. **Numerical simulations and phase diagram.** Our analytical results provide information about local bifurcations. In addition we have performed numerical simulations of the ODEs (18), in order to obtain the full system's picture. As occurred in the previous section, we can assume that α_j are real variables. In addition, we have performed numerical simulations of the original system that indicate that this assumption yields to correct results.

Figure 4 shows the disposition of qualitatively different dynamics in the parameters space spanned by γ and K, for a particular value of ξ. Like in [13] we find that three codimension-two points organize the parameter space: Takens-Bogdanov (A), degenerate pitchfork (B), and Saddle-node separatrix-loop (D)

[31]. The three codimension-two points collapse at $\xi = \gamma = 0$, see Fig. 2, and expressions (29) and (7). Line D approaches the origin linearly: $\xi_D(\gamma \to 0) = a\gamma$ with $a \simeq 0.493$, suspiciously close to $\frac{1}{2}$.

One can better understand Fig. 4 looking at the panels of Fig. 5, in which phase portraits for qualitatively different states are shown. In the rightmost part of Fig. 4, $\gamma > \gamma_B = \xi^{1/3}$, the distribution becomes unimodal, and thus the standard route to partial synchronization is found. In the leftmost part, $\xi \leq \gamma < \gamma_D \simeq 0.59997$ ($K_D \simeq 3.7646$), we have the same route than in the previous section, *i.e.* a SW state limited by Hopf and SNIC bifurcations. In contrast, in the central part of the phase diagram (around point A), there exist two regions with bistability where the observed asymptotic state depends on the initial conditions. In one region (SW/PS) standing waves and partial synchronization coexist, and the SW state (a limit cycle) disappears via a heteroclinic collision with the saddle points born at mirror saddle-node bifurcations. In the second region (I/PS) incoherence and partial synchronization coexist.

Bifurcation lines in Fig. 4 are calculated from analytical results and from numerical integration of the ODEs (18). Empty symbols in the figure show the bifurcations determined integrating the Kuramoto model with $N = 2000$. The agreement is good and confirms the validity of the OA ansatz.

4.2.1. *Codimension-two point A.* In this subsection we make a short digression about the codimension-two point A and the importance of the symmetries in the model. Point A in Fig. 4 is a Takens-Bogdanov point of system (18) that has $O(2)$ symmetry. This stems from the inherent $O(2)$ symmetry of the Kuramoto model [with symmetric $g(\omega)$]. Numerics show that the asymptotic dynamics occurs in the real plane —*i.e.* Eqs. (18) with real coordinates— where the symmetry group is only $Z_2 \subset O(2)$. This symmetry imposes the global bifurcation (Het) to be nontangent to the Hopf line [30], in contrast with a nonsymmetric Takens-Bogdanov point. Two scenarios are possible around the odd-symmetric Takens-Bogdanov point [30]. Hence, one may wonder if the alternative scenario, involving a saddle-node bifurcation of limit-cycles, might also be found in the Kuramoto model.

The scenario that we have presented in this section (see also [13]) is apparently the same one Bonilla *et al.* [15] uncovered in the neighborhood of the Takens-Bogdanov point for the Kuramoto model with additive noise and a bi-delta frequency distribution. In that work the full $O(2)$ symmetry is taken into account. Refs. [12, 15] found that, due to the $O(2)$ symmetry, the degenerate Hopf bifurcation gives rise to a branch of unstable traveling wave solutions, in addition to the stable SW. According to [15] these traveling wave solutions should disappear at a certain $K < K_P$ in a local bifurcation with the saddle fixed points $X_{(1)}$ born at the SN bifurcations. This bifurcation reverses the transversal stability of the saddle fixed points, what in turn makes congruent the pitchfork bifurcation of these fixed points with the completely unstable fixed point at origin. We think

these traveling wave solutions and their associated bifurcations are captured by the reduced Eqs. (18) because the OA ansatz has retained the $O(2)$ symmetry of the model. This means that although the relevant dynamics (the attractors) are inside the real plane of (α_1, α_2), physical unstable objects (traveling waves) "live" outside this plane.

5. Conclusions

We have investigated the routes to synchronization in the Kuramoto model with a bimodal distribution constructed as the difference of two unimodal distributions of different widths. These distributions admit an arbitrarily deep and narrow central dip, what is not achievable in distribution types considered in the past. This has allowed us to reinforce and extend the results recently published in [13].

We have found that bimodal distributions (5) near unimodality produce hysteretic phase transitions, except in some region in the neighborhood of the unimodal limit $(\xi, \gamma) = (0, 0)$, see Fig. 2.

We expect a wide family of bimodal distributions to exhibit the same qualitative features that Fig. 2: The hysteretic region exist at the bimodal side of the unimodal-bimodal border, and it shrinks as the nonregular unimodal-bimodal transition ($g''(0) = \infty$) is approached. Moreover the absence of hysteresis for $g(0) = 0$ should be found in any bimodal distribution if the dependence is quadratic —as in our distribution (5)— or has a larger power: $g(\omega) \propto |\omega|^\nu$ for small ω, with $\nu \geq 2$.

Appendix A. Proof of the transversal stability of fixed point $X_{(2)}$ in Sec. 3

Global phase shift invariance, $(\alpha_1, \alpha_2) \to (\alpha_1 e^{i\beta}, \alpha_2 e^{i\beta})$, allows to reduce Eqs. (18) in one dimension by passing to polar coordinates, $\alpha_j = \rho_j e^{i\phi_j}$, and defining the phase difference $\psi = \phi_1 - \phi_2$. We obtain three ODEs:

$$\dot{\rho}_1 = -\rho_1 + k(\rho_1 - \xi\rho_2 \cos\psi)(1 - \rho_1^2) \tag{31a}$$

$$\dot{\rho}_2 = -\gamma\rho_2 + k(\rho_1 \cos\psi - \xi\rho_2)(1 - \rho_2^2) \tag{31b}$$

$$\rho_1\rho_2\dot{\psi} = -k\left[(1-\xi)\rho_1^2\rho_2^2 + \rho_1^2 - \xi\rho_2^2\right]\sin\psi \tag{31c}$$

In Sec. 3 we took $\xi = \gamma$ and found that twin saddle-node bifurcations (namely SNICs) give rise to two pairs of fixed points. Here we prove (we rather sketch the proof) the transversal stability of the mirror fixed points associated to $X_{(2)}$ via Eq. (21).

First of all note that $X_{(2)}$ yields a fixed point (x_1, x_2), and its mirror image, with x_1 and x_2 having the same sign, $\psi = 0$. This is a consequence of Eq. (21) because $X_{(2)} < 1 - 1/k$. The latter inequality stems from the fact that $Q(1 - 1/k) =$

$-\gamma^2 < 0$ and by continuation of the solutions from $k = \infty$: $\lim_{k\to\infty} X_{(1)}(k) = 0$, $\lim_{k\to\infty} X_{(2,3)}(k) = 1$.

Therefore we have to prove that factor

$$F = (1-\gamma)\rho_1^2\rho_2^2 + \rho_1^2 - \gamma\rho_2^2 \tag{32}$$

in Eq. (31c) for $\dot{\psi}$ is positive. Replacing $\rho_1^2 = X_{(2)}$ and $\rho_2^2 = X_{(2)} + 1/k$, we have

$$F = (1-\gamma)[X_{(2)}^2 + X_{(2)}(1+1/k)] - \gamma/k. \tag{33}$$

As $X_{(2)}$ exists only above the saddle-node bifurcation ($k \geq k_{SN}$) and $k_{SN} > k_H = (1+\gamma)/(1-\gamma)$.

$$F > (1-\gamma)h \tag{34}$$

with

$$h = X_{(2)}^2 + X_{(2)} - \gamma/(1+\gamma). \tag{35}$$

Then $h > 0$ is a sufficient condition for the transversal stability of the fixed point.

It suffices to prove that h is positive at the locus of the saddle-node bifurcation because $X_{(2)}(k,\gamma)$ exhibits its minimal value over k precisely at the bifurcation: $X_{(2)}(k > k_{SN}, \gamma) > X_{(2)}(k_{SN}, \gamma)$. For our aim it is better to parameterize the SNIC line by k instead of γ. Hence we to introduce in (35) the expressions

(i) γ as a function of k_{SN}, via Eq. (26).
(ii) $X_{(2)}(k_{SN})$, determined from (25) in the two-fold root case.

The calculation of terms (i) and (ii) can be readily done with symbolic software such as MATHEMATICA. As a result we obtain a function $h(k_{SN})$ that is positive in all the domain of $k_{SN} \in (1, \infty)$.

Moreover using expressions (27) and (28) we can get approximate expression for h (as a function of γ):

$$h(\gamma \to 0) = \left(\frac{\gamma}{2}\right)^{2/3} + O(\gamma) \tag{36}$$

$$h(\gamma \to 1) \simeq 0.0858 \tag{37}$$

Appendix B. Stability of the incoherent state in the Kuramoto model with noise

For the sake of completeness, and as a double-check of some of the results obtained, we study here the stability of the incoherent state when the model is perturbed with additive white noises. In this case, the right hand side of Eq. (1) has to be supplemented with uncorrelated fluctuating terms η_i satisfying $\langle \eta_i(t)\eta_j(t')\rangle = 2\sigma\delta_{ij}\delta(t-t')$. So far a counterpart of the Ott-Antonsen ansatz for the stochastic problem has not been found. It is nonetheless possible to obtain the

stability boundary of incoherence resorting to the Strogatz and Mirollo relation for the discrete spectrum of eigenvalues λ [21]:

$$\frac{K}{2}\int_{-\infty}^{\infty}\frac{g(\omega)}{\lambda+\sigma+i\omega}d\omega=1. \tag{38}$$

Considering the distribution of frequencies (5), this equation can be solved for the eigenvalues λ.

Noise increases the domain of the incoherent state. Hopf and pitchfork bifurcations continue to occur, but the values of K are shifted to larger values. We obtain:

$$K_H = 2+2\gamma+4\sigma \tag{39}$$

$$K_P = \frac{2(\gamma+\sigma)(1-\xi)(1+\sigma)}{(\gamma-\xi)+\sigma(1-\xi)}, \tag{40}$$

that indeed reduce to Eqs. (24) and (30) for $\sigma=0$. The location of the Takens-Bogdanov point [c.f. Eq. (29)] also varies and now pitchfork and Hopf bifurcations collide ($K_H=K_P$) at :

$$\xi_A=\left(\frac{\gamma+\sigma}{1+\sigma}\right)^2. \tag{41}$$

References

[1] A. S. Pikovsky, M. G. Rosenblum, and J. Kurths, *Synchronization, a Universal Concept in Nonlinear Sciences.* (Cambridge University Press, Cambridge, 2001).
[2] A. T. Winfree, *The Geometry of Biological Time* (Springer, New York, 1980).
[3] L. Glass, and M. C. Mackey, *From Clocks to Chaos: The Rhythms of Life* (Princeton University Press, NJ, 1988)
[4] J. Dye, J. Comp. Physiol. A **168**, 521 (1991).
[5] J. Buck, Q. Rev. Biol. **63**, 265 (1988).
[6] A. Sherman, and J. Rinzel, Biophys. J. **59**, 547 (1991).
[7] S. H. Strogatz, D. M. Abrams, A. McRobie, B. Eckhardt, and E. Ott, Nature **438**, 43 (2005).
[8] Y. Kuramoto, *Chemical Oscillations, Waves, and Turbulence* (Springer-Verlag, Berlin, 1984).
[9] S. H. Strogatz, Physica D **143**, 1 (2000).
[10] S. C. Manrubia, S. S. Mikhailov, and D. H. Zanette, *Emergence of Dynamical Order* (World Scientific, Singapore, 2004).
[11] J. A. Acebrón *et al.*, Rev. Mod. Phys. **77**, 137 (2005).
[12] J. D. Crawford, J. Stat. Phys. **74**, 1047 (1994).
[13] E. A. Martens *et al.*, Phys. Rev. E **79**, 026204 (2009).
[14] L. L. Bonilla, J. C. Neu, and R. Spigler, J. Stat. Phys. **67**, 313 (1992).
[15] L. L. Bonilla, C. J. Pérez-Vicente, and R. Spigler, Physica D **113**, 79 (1998).
[16] L. L. Bonilla, Phys. Rev. E **62**, 4862 (2000).
[17] E. Montbrió, D. Pazó, and J. Schmidt, Phys. Rev. E **74**, 056201 (2006).
[18] H. Okuda and Y. Kuramoto, Prog. Theor. Phys. **86**, 1159 (1991).
[19] E. Montbrió, J. Kurths, and B. Blasius, Phys. Rev. E **70**, 056125 (2004).
[20] E. Barreto, B. Hunt, E. Ott, and P. So, Phys. Rev. E **77**, 036107 (2008).

[21] S. H. Strogatz and R. E. Mirollo, J. Stat. Phys. **63**, 613 (1991).
[22] E. Ott and T. M. Antonsen, Chaos **18**, 037113 (2008).
[23] L. M.Childs and S. H. Strogatz, Chaos **18**, 043128 (2008).
[24] T. M. Antonsen *et al.*, Chaos **18**, 037112 (2008).
[25] D. W. Abrams, R. Mirollo, and S. H. Strogatz, Phys. Rev. Lett. **101**, 084103 (2008).
[26] C. R. Laing, Chaos **19**, 013113 (2009).
[27] W. Shing Lee, E. Ott, and T. M. Strogatz, Phys. Rev. Lett. **103**, 044101 (2009).
[28] E. Ott and T. M. Antonsen, Chaos **19**, 023117 (2009).
[29] A. Pikovsky and M. Rosenblum, Phys. Rev. Lett. **101**, 264103 (2008)
[30] J. Guckenheimer and P. Holmes, *Nonlinear Oscillations, Dynamical Systems, and Bifurcations of Vector Fields* (Springer-Verlag, New York, 1983).
[31] S. Schecter, SIAM J. Math. Anal. **18**, 1142 (1987).

Diego Pazó
Instituto de Física de Cantabria (IFCA)
CSIC-Universidad de Cantabria
E-39005 Santander, Spain

Ernest Montbrió
Computational Neuroscience Group
Department of Information and Communication Technologies
Universitat Pompeu Fabra
08003 Barcelona, Spain

Center for Neural Science
New York University
New York, NY 10012, USA